Josephson current for a Graphene nanoribbon using a lattice model

Somayyeh Zareei [1], Vahid Daadmehr [1*], Hossein Hakimi Pajouh [1], and Zahra Faraei [2]

[1]*Magnet & superconducting Res. Lab., Department of Physics, Alzahra University, Tehran, 199389, I.R. Iran*

[2] *Department of Physics, Sharif University of Technology, Tehran, I.R. Iran*

ABSTRACT

A tight binding approach based on the Bogoliubov de-Genes approach has been used to calculate the DC Josephson current for short junctions with respect to the superconducting coherence length with a lattice model for S-GNR-S junctions. We calculate the phase, length, width, and chemical potential dependence at the Josephson junction and discuss the similarities and differences with regard to the theoretical and experimental results obtained for graphene. Regarding the calculations on graphene, using a lattice model, we convert the graphene honeycomb structure to a brick lattice structure that does not change the lattice topology. Then, by removing several atoms from the lattice, we create the simple vacancy defects in the brick lattice. Also we calculate the Josephson current with these vacancies.

1 Introduction

Graphene, first discovered in 2004, is a thick atomic sheet of sp^2 - bonded carbon atoms. Since then, researchers around the world have been interested in graphene for the interconnect application in submicron regions. Graphene is a semiconductor with zero band gap, phonon like 2D confined properties, linear energy dispersion, and a very high mobility of carriers $(10^4 cm/Vs)$ at room temperature [1].

Due to its zero energy gap, graphene cannot be used directly to make transistor devices, but it can be used for the logic applications. So, a further confinement of the electrons of graphene in one of the in plane directions will allow for broader applications. These graphene ribbons are strips of graphene with dimensions less than ten nanometers, so it is called

graphene nanoribbons (GNR) [1]. GNR can depending upon their termination style be two types of armchair and zigzag. The width of armchair GNR is decided by the number of hexagonal carbon rings, so it is indicated by dimer lines (Na) across the ribbon. Similarly the width of zigzag GNR is dependent on the number of zigzag chains (Nz) across the ribbon [2].

These termination styles are one of the factors in determining electronic states of GNRs. According to the tight binding model, zigzag GNRs are metallic and armchair. GNRs that are either metallic or semiconducting are further dependent on their width [3]. Band structure calculations show that the armchair GNRs with ideal edges are semiconducting when the number of dimer lines is 3Na or (3Na+1), and when the number of dimer lines is (3Na+2) they are metallic. Zigzag GNRs are independent of N and have a metallic behavior [4]. The results of DFT calculation

show that armchair GNRs are semiconductors with energy gaps where their energy gap is inversely dependent on the GNR width [2].

Owing to the proximity effect, in contact of graphene with superconductor, a superconductor can also induce non zero pairing potential in the graphene. With having such graphene and superconductor hybrid structures, in particular the Andreev reflection taking place at the graphene- superconductor interface, the subject was first studied theoretically by Titov and Beenakker [5], for a review on Andreev reflection in graphene see Ref [6]. Using a Dirac Bogoliubov de Genes (DBdG) formalism, they found that in a ballistic graphene, a Josephson current can flow at the Dirac point even in the limit of zero concentration of the carriers. In fact, the proximation of superconductor with graphene induces an unusual coherent superconducting order in the nearest layers of graphene in the interface which is often a result of the physical characteristic of graphene in the normal state. The Josephson effect in junctions SNS (S: superconductor, N: normal metal or semiconductor) occurs due to the phase coherence of electron and hole in the normal region. When an electron is scattered into a hole at an SN interface (Andreev reflection), it acquires a phase displacement proportional to the phase of the superconducting order parameter. Thus the electronic states of the SNS junction depend on the difference between the phase of two closely spaced left and right superconductors (φ), which is the origin of the DC Josephson effect: $I = -dF/d\varphi$ (I: current; F: free energy).

Therefore, the DC Josephson effect is sensitive to the nature of electronic transport in the normal region, and we can expect that the Josephson current in a SNS junction shows some similar effects, such as the universal fluctuations of conductance and the conductance quantization, in mesoscopic systems. The normal region is of the mesoscopic size while the superconductors are very large and they are considered as bulk. In fact, the fluctuations of the critical current in dirty SNS junctions have been analyzed theoretically [7] and also observed experimentally [8].

For transport in the normal conductor, there must be present phase coherent and time reversal symmetry (TRS). In graphene, the Josephson's effect can be investigated in the 'relativistic' regime [5], where the supercurrent is carried by Dirac electrons. It has also been shown experimentally that Josephson's effect in graphene is a robust effect and its robustness is linked to graphene's unique electronic structure [9].

Using theoretical calculations on the Josephson current passing through the graphene, a current – phase relationship is obtained as:

$$I(\varphi) \propto \cos(\varphi/2)\arctan h(\sin(\varphi/2)),$$

where a critical current depends inversely on the length of the junction L (L is the distance between two superconductors) [10]. Experimentally the proximity induced superconductivity in graphene was observed by Heersche et al [11] for first time and later by others [12-15] which is acquired by superconducting connections investigation in a graphene sheet which leads to transport properties of graphene. Some of the key findings in these investigations include the possibility of specular Andreev reflection, oscillations in the conductance of a superconductor-normal (SN) junction, and a finite Josephson current even at the Dirac point in a superconductor – normal-superconductor (SNS) junction. So far often in papers, the conventional s-wave superconducting pairing has been made; while only a little attention has been paid to the unconventional pairing that affects the transportation properties [16]. We calculate numerically the Josephson current for a metal armchair nanoribbon (A GNR) in brick lattice. To do this, we generalize the Furusaki method [19] for a honey comb lattice to a brick lattice. The advantage of the numerical method employed here is that we can examine the effect of impurities and point vacancy defects in different quantities and arrays.

2 Theory

The Josephson junction is described by the Bogoliubov–de Genes equation [17] on the two dimensional tight binding model. The Josephson current is represented by the Matsubara Green function which is numerically calculated by using the recursive Green function method [18]. The advantage of the method is due to its wide applicability to various systems such as the clean (ballistic) junctions, the dirty (diffusive) junctions, and the junctions in the localized regime. Let us consider the *SNS* junction (Fig 1) on the

two-dimensional tight-binding model, where the length of the normal segment is La_0 and the width of the junction is Wa_0 where a_0 is the lattice constant.

For this simple two-dimensional lattice, the Hamiltonian is assumed to be:

$$H = -t\sum_{\sigma}(\sum_{j=-\infty}^{\infty}\sum_{k=0}^{n_y}(c_{j,k,\sigma}^{\dagger}c_{j-1,k,\sigma}+c_{j-1,k,\sigma}^{\dagger}c_{j,k,\sigma})$$

$$+\sum_{j=1}^{n_x}\sum_{k=0}^{n_y}\sum_{\sigma}\varepsilon_{j,k}c_{j,k,\sigma}^{\dagger}c_{j,k,\sigma}-\mu\sum_{j=-\infty}^{\infty}\sum_{k=0}^{n_y}c_{j,k,\sigma}^{\dagger}c_{j,k,\sigma}\ ,(1)$$

$$-\sum_{j=-\infty}^{\infty}\sum_{k=0}^{n_y}(\Delta_{j,k}c_{j,k,\downarrow}^{\dagger}c_{j,k,\uparrow}^{\dagger}+\Delta^{*}c_{j,k,\uparrow}c_{j,k,\downarrow})$$

Where $c_{j,k,\sigma}$ is an annihilation operator of an electron on site (j,k) with spin σ. Here, j is cells counter in horizontal direction and k is cells counter in vertical direction. t is a hopping matrix element and μ is the chemical potential. The system has wire geometry (meaning the width is limited) where the number of places in the transverse direction is $n_y + 1$ and we take the number of unit cells in the horizontal direction for the normal region as n_x. It is assumed that the order parameter $\Delta_{j,k}$ is in the left superconductor, in the region $j \leq 0$, as Δ_L, and in the right superconductor, in the region $j \geq n_x + 1$, as $\Delta_R \exp(i\varphi)$, where φ is the phase factor.

Josephson current is obtained using two - particle Green function as following:

$$I = -\frac{iet}{\hbar}\sum_{\sigma}\sum_{k=0}^{n_y}\langle c_{j,k,\sigma}^{\dagger}c_{j+1,k,\sigma}-c_{j+1,k,\sigma}^{\dagger}c_{j,k,\sigma}\rangle$$

$$=\frac{iet}{\beta\hbar}\sum_{\omega_n}\sum_{k=0}^{n_y}\text{Tr}[G_{\omega_n}(j,k;j+1,k)-G_{\omega_n}(j+1,k;j,k)]\ ,(2)$$

Where < …. > means thermal average, β is the inverse temperature, and $G_{\omega_n}(j,k;j',k')$ is the Nambu Green Function (2×2 matrix) with the Matsubara frequency $\omega_n = \pi k_B T(2n+1)$. The Green function satisfies the equation of motion:

$$\begin{pmatrix} i\omega_n - H_{j,k} & -\Delta_{j,k} \\ -\Delta_{j,k}^* & i\omega_n + H_{j,k}^* \end{pmatrix} G_{\omega_n}(j,k;j',k') = \delta_{j,j'}\delta_{k,k'}\ ,(3)$$

where we have $H_{j,k} = -t(d_{-x}+d_{+x})+\varepsilon_{j,k}-\mu$, and d_e is a hopping operator which shifts the site (j,k) by one lattice spacing in the e-direction. Equation (3) can be solved with the cursive Green function method [19]. As given in reference [19], the Green's function can be calculated separately for each region (the left superconductor, the normal region, the right superconductor). Then, the Green function of the connected system is obtained which is needed for calculating the Josephson current.

We start from the left superconductor ($j \leq 0$) which is not connected to the normal region in the beginning (Fig 1).
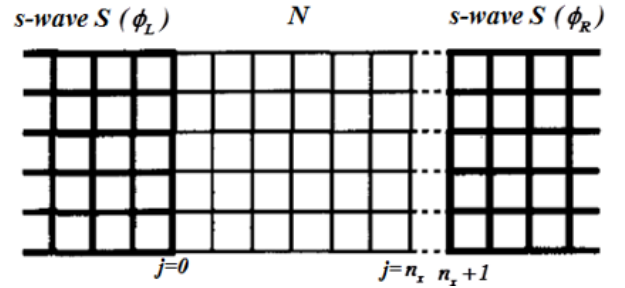

Figure 1. Schematics of the SNS junction.

The Green function in the edge of the left superconductor is given by:

$$G_{\omega_n}(0,k;0,k') = \sum_{m=1}^{n_y+1}\frac{e^{ip_{m,L}^+}}{t_h\Omega_{n,L}(n_y+2)}\sin[q_m(k+1)]$$

$$\sin[q_m(k'+1)]\times\begin{pmatrix}-\Omega_{n,L}-\omega_n & i\Delta_L \\ i\Delta_L & \Omega_{n,L}-\omega_n\end{pmatrix}$$

$$-\sum_{m=1}^{n_y+1}\frac{e^{-ip_{m,L}}}{t_h\Omega_{n,L}(n_y+2)}\sin[q_m(k+1)]\sin[q_m(k'+1)]$$

$$\times\begin{pmatrix}\Omega_{n,L}-\omega_n & i\Delta_L \\ i\Delta_L & -\Omega_{n,L}-\omega_n\end{pmatrix}\ ,(4)$$

Where we have

$$\Omega_{n,L(R)} = \sqrt{\omega_n^2 + \Delta_{L(R)}^2} \ , \quad q_m = m\pi / (n_y + 2) \ ,$$

and

$$p_{m,L(R)}^{\pm} = \arccos[-(\mu + 2t_h \cos q_m \pm \Omega_{n,L(R)})/2t_h] \ .$$

Next we separate the normal region into cells in such a way that the cell j consists of the sits (j,k) (k=0,…….., ny) and attach the cells to the left superconductor one by one, see Fig 1.

To perform calculations on graphene, we can convert the graphene-shaped honeycomb lattice structure into a brick lattice structure which does not change the lattice topology [20] (Fig 2). In this model, the direction of each bond is aligned with two perpendicular axes. This transformation can be considered as a distorted honeycomb lattice under the influence of compression in $\hat{y}$ direction together with extension in $\hat{x}$ direction. On the other hand, if we consider the energy dispersion relation for graphene which has a honeycomb shape and compare it with the relation obtained for the brick lattice, as given in reference [20], it can be seen that the same result has been obtained. The topology of brick-type lattice is still similar to the honeycomb lattice but with different lattice vectors. In addition, the probability of jump between two adjacent cells is independent of the shape of the lattice.
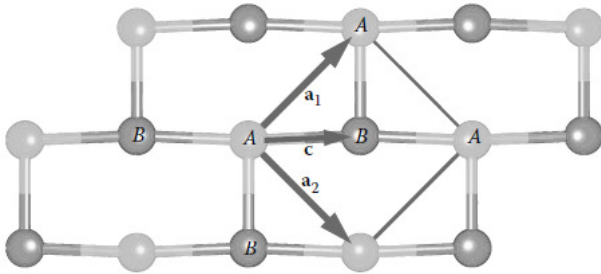

Figure 2. Crystal structure of brick-type lattice that is a transformation from honeycomb lattice showing sub lattices *A* and *B* in the unit cell and the basis vector **c**. The primitive unit cell is defined by the primitive lattice vectors a1 and a2.

In Ref [19], for a square lattice, the hopping matrix from one cell to the adjacent cell (t) in the horizontal and vertical directions is the same, but by changing the lattice to a brick lattice, we define the hopping matrix

from a cell to the adjacent cell in a horizontal direction t_h and in a vertical direction t_v, where is in the vertical direction as one in between (Fig 3).
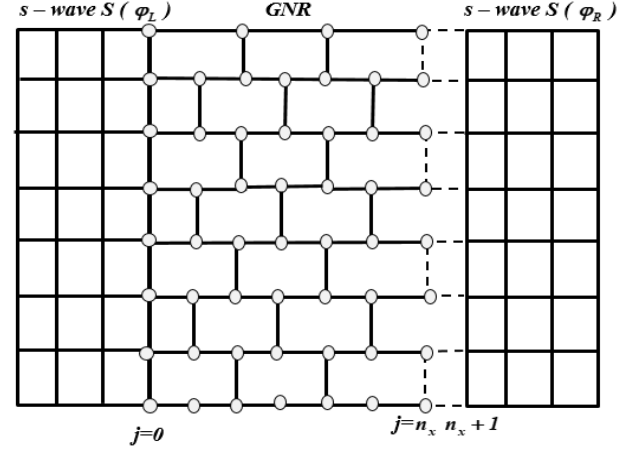

Figure 3. Schematic diagram of the superconductor – graphene nanoribbon - superconductor, in which the graphene nanoribbon has become a brick lattice.

In the Furusaki method, the middle region is considered a square lattice but in our work, with the deformation of the middle region, the Green's function in this region must be changed. We will generalize the relationships to the brick lattice by changing the Hamiltonian matrix given for each cell and changing the hopping matrix from one cell to the adjacent cell, as follows:

$$G_{\omega_n}(j,k;j',k') = [i\omega_n \delta_{k,k'} I - H_j(k,k') \\ -H' G_{\omega_n}(j-1,k;j-1,k')H']^{-1} \quad , (5)$$

$$H_j(k,k') = \begin{pmatrix} H_0 & 0 \\ 0 & -H_0^* \end{pmatrix}$$

where

$$H_0 = -t_v(\delta_{k,k'-1} + \delta_{k,k'+1}) + (\varepsilon_{j,k} - \mu)\delta_{k,k'} \ ,$$

and

$$H' = -t_h \begin{pmatrix} 1 & 0 \\ 0 & -1 \end{pmatrix}.$$

Finally we attach the right superconductor to the semi-infinite SN system. To this end we need the Green function for the right superconductor:

$$G_{\omega_n}(n_x+1,k;n_x+1,k') = \sum_{m=1}^{n_y+1} \frac{e^{jp_{m,L}^+}}{t_h \Omega_{n,R}(n_y+2)} \sin[q_n$$

$$\sin[q_m(k'+1)] \times \begin{pmatrix} -(\Omega_{n,R}+\omega_n) & i\Delta_R e^{i\varphi} \\ i\Delta_R e^{-i\varphi} & \Omega_{n,R}-\omega_n \end{pmatrix}$$

$$-\sum_{m=1}^{n_y+1} \frac{e^{-ip_{m,R}^-}}{t_h \Omega_{n,R}(n_y+2)} \sin[q_m(k+1)] \qquad .(6)$$

$$\sin[q_m(k'+1)] \times \begin{pmatrix} \Omega_{n,R}-\omega_n & i\Delta_R e^{i\varphi} \\ i\Delta_R e^{-i\varphi} & -(\Omega_{n,R}+\omega_n) \end{pmatrix}$$

Then the Green function of the connected system is obtained from the following two equations:

$$G_{\omega_n}(n_x,k;n_x+1,k') = \sum_{l=0}^{n_y} \{[G_{\omega_n}(n_x,k;n_x,l)]^{-1}$$

$$-H'G_{\omega_n}(n_x+1,k;n_x+1,k')H'\}^{-1} \times H'G_{\omega_n}(n_x+1,l;n_x+1,k')$$

$$G_{\omega_n}(n_x+1,k;n_x,k') == \sum_{l=0}^{n_y} G_{\omega_n}(n_x+1,k;n_x+1,l)H' \qquad ,(7)$$

$$\{[G_{\omega_n}(n_x,l;n_x,k')]^{-1} - H'G_{\omega_n}(n_x+1,k;n_x+1,k')H'\}^{-1}$$

The Josephson current is calculated from equations (2) and (7).

3 Results and Discussion

In this section, we present the numerical results for Josephson current by using the lattice model that was introduced in the previous section. Figure 4 shows the dependence of the Josephson current on the width of the junction (W) and a little chemical potential value ($\mu_n = 0.001ev$) for a metal armchair ribbon with a length of $L = 50a_{c-c}$ ($a_{c-c} = 0.142nm$). When $\mu_n \to 0$, the available propagating modes decrease, where the results are in agreement with the results of Ref [21]. Josephson current has linear dependence on W and with increasing the band width, Josephson current also rises. This behavior is the result of a quasi-diffusion transport in a ballistic graphene [22]. By decreasing W/L, transmission of transverse modes from the normal region decreases and the current shows a uniform decrease.
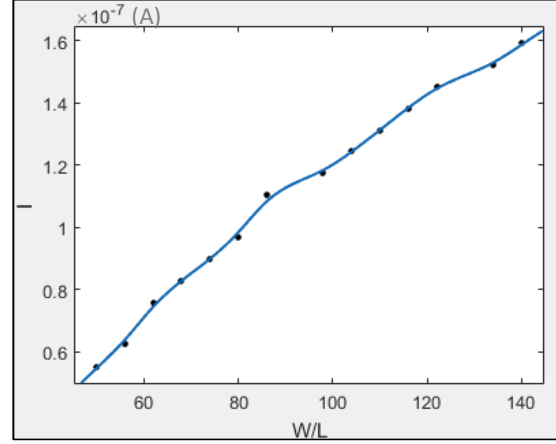

Figure 4. Curve of Josephson current in terms of ribbon width.

In the graphene-superconductor interface, edges states extend from one boundary to another along the interface and the Andreev reflection occurs. With widening of the graphene ribbon, edge states of electron and hole are also combined together. Thus, the probability of the Andreev reflection also increases. Figure 5 shows the dependence of the Josephson current on the chemical potential in the ribbon width $W = 86a_{c-c}$ and the length of the junction $L = 50a_{c-c}$. In fact, we have assumed in our calculations that superconducting regions are doped so that $\mu_s \gg \mu_n$. As the chemical potential increases, the Josephson current also increases linearly. In other words, by decreasing μ_n, the current also decreases; when $\mu_n \to 0$, the available propagating modes decrease which is consistent with the prediction reported in Ref [23].

In this section, we investigate the dependence of the Josephson current on the length of the junction (L) in the short junction region ($L \ll \xi$ that $\xi = \dfrac{\hbar v_F}{\Delta_0}$) which is shown in Fig 6.

In the vicinity of the Dirac point, we can see oscillations in curve I in terms of L and that simultaneously the current decreases exponentially.
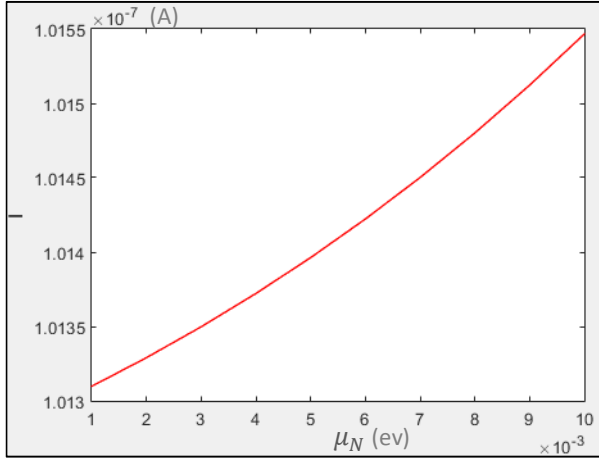
Figure 5. Curve of Josephson current versus chemical potential in Josephson junction.

However, we cannot see the current dependence behaving as $\approx 1/L^2$ which has been predicted in Ref [24] for $L \ll \xi$. It should be noted that an increase in the GNR's length causes an increase in the number of Andreev levels and hence decreases the current; because the number of Andreev bound states has a relation proportional to the length of the junction (L) [25].
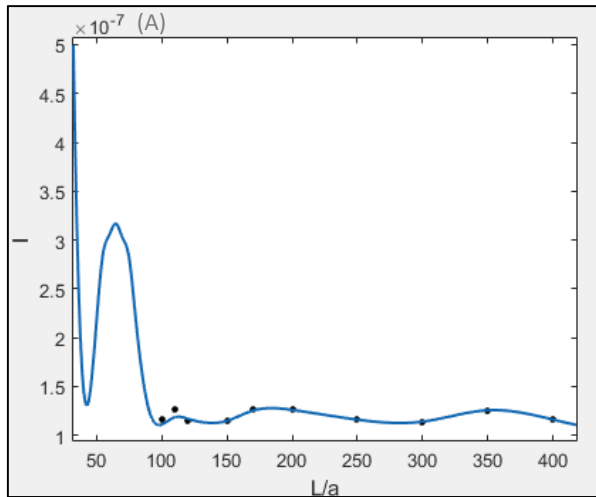

Figure 6. Curve of Josephson current versus length of junction in short junction region ($L << \xi$).

Key information about processes that involve in Josephson current not only can be obtained by measuring the magnitude of the Josephson current but also by measuring the phase difference between two superconductors placed at both sides of the nano

ribbon which is characterized by the Josephson current phase (CPR) relationship. Figure 7(a) shows the Josephson current as a function of the phase difference φ for a short junction ($L \ll \xi$) in three temperatures $T / T_C = 0.4, 0.53, 0.7$, for $L = 50a_{c-c}$ and $W = 68a_{c-c}$. As seen from Fig 7 (a), by increasing the temperature, the maximum current is reduced.
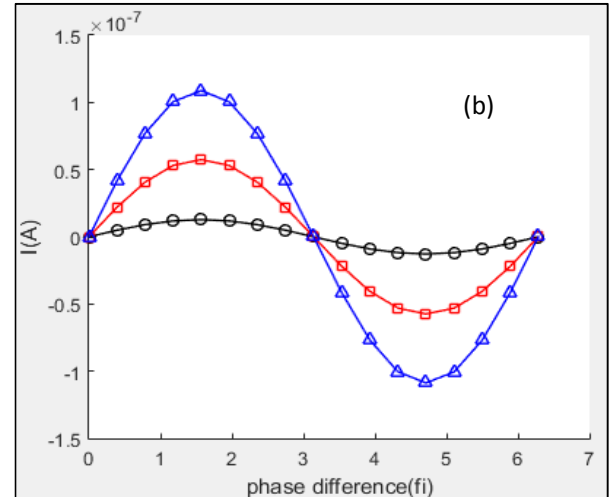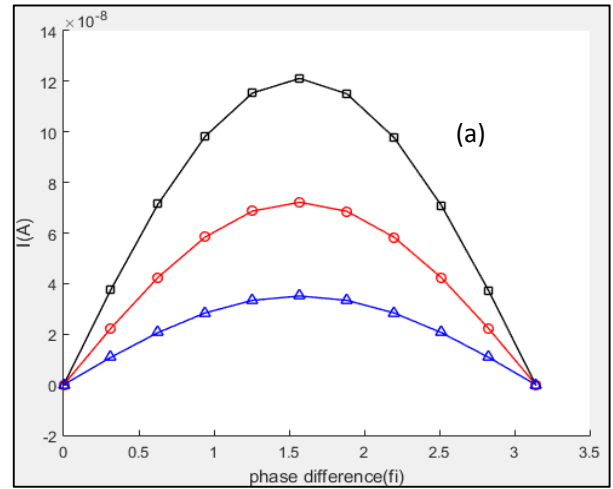

Figure 7. (a) Curve of Josephson current versus phase difference φ for a short junction ($L \ll \xi$) in three temperature region , $T / T_C = 0.4, 0.53, 0.7$ (respectively black □ , red ○ and blue △). (b) Phase – current relationship for Josephson junction for three ratios W/L=10, 1, 0.1 (respectively blue △ , red □ and black ○).

At high temperatures, the current shows a simple sinusoidal dependence on the phase; while at low temperatures, the position of the maximum current, as a result of the asymmetry in the curves, moves very slight, slightly to the right. By following Ref [26], this

asymmetry is defined by the relation $s = (2\phi_{max}/\pi) - 1$ that ϕ_{max} is the maximum current position.

Figure 7 (b) also shows the phase dependence of the Josephson current for a metal armchair ribbon for three ratios of W / L = 10, 1, 0.1. For a short Josephson junction, the relationship of the current in terms of the phase difference is sinusoidal-shaped, $I(\phi) = I_C \sin\phi$, similar to a tunneling Josephson junction. It is expected that at this level of junction length, transmission probabilities are very small and graphene ribbons behave like a tunneling junction [27]. As shown in Fig 6 (b), whatever the ratio of the width to the ribbon length is greater, the maximum current is also greater, which is the same as the result obtained from curve 4, in which it was shown that I has linear dependence on W / L.
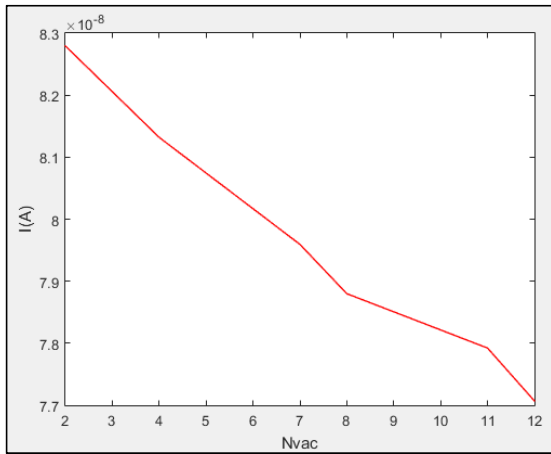

Figure 8. Curve of Josephson current versus the number of vacancies in a graphene nanoribbon lattice, which shows that Josephson current decreases with the number of vacancies.

Now, after ensuring our computational approach, by removing an atom from the lattice, we create a simple vacancy in the brick lattice. When there is a vacancy in the ribbon, the number of conducting channels decreases. The appearance of these vacancies changes the green function of graphene; because, removing each atom, a vertical hopping (t_v) and two horizontal hopping (t_h) are eliminated. This change affects the Josephson's current, and, as shown in Fig 8, the Josephson current decreases with increasing the number of vacancies in the lattice.
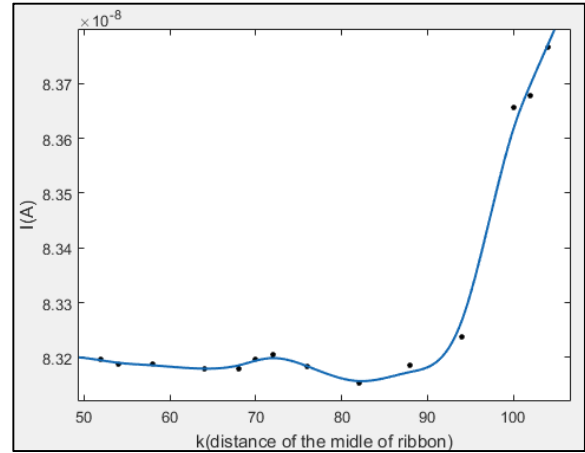

Figure 9. curve of Josephson current versus the position of vacancies in a graphene nanoribbon lattice, when the vacancies move from center to edge of ribbon.

Then we consider a graphene nanoribbon lattice with 5 vacancies, where the position of these vacancies moves from center to edge of the ribbon. We study the Josephson current in the appearance of these vacancies. Figure 9 shows the Josephson current in terms of the position of these vacancies. As seen in Fig 9, the Josephson current has the lowest value when the vacancies are in the middle of the ribbon and as they move towards the edge of the ribbon, it increase.

By removing one atom from the lattice of the graphene ribbon, three sp^2 bonds are broken, creating three dangling bonds at the neighboring carbon atoms. These dangling bonds tend to spread towards the neighboring carbon atoms of the ribbon in order to overlap with electronic states of their neighbors where their energy is less. Hence, the electronic wave functions near the created vacancy are affected. In other words, some localized states appear in the vicinity of the vacancy and affect the π bonds of the ribbon. Therefore, the effect of the vacancy on the π bands, which are responsible for conduction near the Fermi energy and hence the Josephson current, is significant. If the localized vacancy states are in the middle of the ribbon, their effect on whole electronic wave function will be maximum. When the vacancy is moved towards one edge, the effect of the localized vacancy states near the other edge will decrease, due to the distance between the vacancy and the increase of the other edge of the ribbon.

Acknowledgments

References

[1] S. Duttaa and S. K. Pati, "Novel properties of graphene nanoribbons: a review." Journal of Materials Chemistry, **20** (2010) 8207.

[2] E. Kan, Z. Li and J. Yang, "Graphene nanoribbons: geometric, electronic, and magnetic properties," Physics and Applications of Graphene, Intech open journal, pp. 331-348, (2011).

[3] S. Rakheja, V. Kumar, and A. Naeemi, "Evaluation of the potential performance of graphene nano-ribbons as On-chip interconnects", contributed paper, proceedings of IEEE, **101** (2013) 1740.

[4] C. Xu, H. Li, and K. Banerjee, "modeling, analysis, and design of graphene nanoribbon interconnects," IEEE transactions on electron devices, **56** (2009) 1567.

[5] C. W. J. Beenakker, "Specular Andreev reflection in graphene." Physical Review Letters, **97** (2006) 067007.

[6] C. W. J. Beenakker, "Andreev reflection and Klein tunneling in graphene." Review Modern Physics, **80** (2008) 1337.

[7] C.W.J.Beenakker," Universal limit of critical-current fluctuations in mesoscopic Josephson junctions." Physical Review Letters, **68** (1992) 1442.

[8] P. Dubos, H. Courtois, B. Pannetier, F. K. Wilhelm, A. D. Zaikin, and G. Schön, "Josephson critical current in a long mesoscopic S-N-S junction", Physical Review B **63** (2001) 064502.

[9] H. B. Heersche, P. Jarillo-Herrero, J. B. Oostinga, L. M. K. Vandersypen, and A. F. Morpurgo, "Bipolar supercurrent in graphene." Nature **446** (2007) 56.

[10] A.G Moghaddam, M Zareyan, "Graphene-based superconducting quantum point contacts." Applied Physics A, **89** (2007) 579.

[11] H. B. Heersche, P. Jarillo-Herrero, "Bipolar supercurrent in grapheme." Nature **446** (2007) 56.

[12] F. Miao, S. Wijeratne, Y. Zhang, U. C. Coskun, W. Bao, and C.N. Lau, "Phase-coherent transport in graphene quantum billiards." Science **317** (2007) 1530.

[13] A. Shailos, W. Nativel, A. Kasumov, C. Collet, M. Ferrier, S.Guéron, R. Deblock , and H. Bouchiat, "Proximity effect and multiple Andreev reflections in few-layer graphene ." Euro Physics Letters, **79** (2007) 57008.

[14] X. Du, I. Skachko, and E. Y. Andrei, "Josephson current and multiple Andreev reflections in graphene SNS junctions." Physical Review B **77** (2008) 184507.

[15] C. Ojeda-Aristizabal, M. Ferrier, S. Guéron, and H. Bouchiat, "Tuning the proximity effect in a superconductor – graphene - superconductor junction." Physical Review B **79** (2009) 165436.

[16] J.Linder, A.M.Black-Schaffer, T.Yokoyama, S.Doniach, and A.Sudbø, "Josephson current in graphene: Role of unconventional pairing symmetries." Physical Review B **80** (2009) 094522.

[17] P.G. de Gennes, "Superconductivity of Metals and Alloys." Published by Benjamin, New York, 1966.

[18] P.A. Lee and D.S. Fisher, "Anderson Localization in Two Dimensions." Physical Review Letters **47** (1981) 882.

[19] A.Furusaki, "DC Josephson effect in dirty SNS junctions: Numerical study ", Physica B **203** (1994) 214.

[20] K. Wakabayashi, M.Fujita, H. Ajiki and M.Sigrist, "electronic and magnetic properties of nanographite ribbons." Physical Review B, **59** (1999) 12.

[21] Qing-feng Sun and X C Xie, "Quantum transport through a graphene nanoribbon–superconductor junction ", Journal of Physics: Condensed Matter, **21** (2009) 344204.

[22] M. Titov and C. W. J. Beenakker, "Josephson effect in ballistic graphene." Physical Review B, **74** (2006) 041401.

[23] H. B. Heersche, P. Jarillo-Herrero, J. B. Oostinga, L. M. K.Vandersypen , and A. F. Morpurgo, " Bipolar supercurrent in grapheme." Nature, **446** (2007) 56.

[24] J. González and E. Perfetto, "Critical currents in graphene Josephson junctions." Journal of Physics: Condensed Matter, **20** (2008) 145218.

[25] L.Qifeng, D.Jinming, "Superconducting switch made of graphene-nanoribbon junctions." Nanotechnology, **19** (2008) 355706.

[26] C. Chialvo, I. C. Moraru, D. J. V. Harlingen, and N. Mason," Current-phase relation of graphene Josephson junctions." ArXiv: 1005.2630v1 (2010).